I R A M P
5(1), June 2014, pp. 23-31

ISSN: 2229-3159

Measurement of Hydrogen Emission Lines Following Pulsed Laser Ablation in Different Ambient Conditions

ASHRAF M. EL SHERBINI[1], DAVID M. SURMICK[2], GHANESHWAR GAUTAM[2], AND CHRISTIAN G. PARIGGER[2,3]

[1]Laboratory of Laser and New Materials, Faculty of Science, Cairo University, Giza, Egypt
[2]The University of Tennessee / UT Space Institute, Center for Laser Applications, 411 B.H. Goethert Parkway Tullahoma, TN 37388-9700, USA, [3]E-mail: cparigge@tennessee.edu

ABSTRACT: Experimental studies of laser ablation with several nanosecond Nd:YAG infrared laser pulses in air frequently reveal hydrogen Balmer series lines due to residual moisture in laboratory environments. For each laser ablation event, capture of the entire emission spectrum from 200 nm to 1000 nm allows us to record data specifically in the wavelength regions of the hydrogen Balmer series members H_α, H_β, H_γ, and H_δ. Here we report the results of measurements of the plasma electron density utilizing the hydrogen lines. The reported values are compared with the results from the optically thin ionic aluminum line at 281.62 nm. The electron density determinations utilize different methods, one by comparison of the spectral line shapes with Voigt profiles of known parameters and the other by evaluation of the peak separation of the beta line at 486.14 nm. The dip feature of the hydrogen beta is clearly developed as the ambient water concentration is increased from normal laboratory moisture to water vapor or when introducing a thin layer of ice at the surface of the aluminum target. The results of the two different analysis methods agree within error margins and also agree with the reference values of the electron density that were obtained from the ionic Al II line.

Keywords: Laser Plasma, Line Strengths, Atomic and Molecular Spectra, Laser Ablation

PACS: 52.50.Jm, 52.25.Os, 32.70.Fw, 32.30.-r, 33.20.-t

1. INTRODUCTION

Time resolved optical emission spectroscopy (OES) of selected species in laser-induced plasma allows one to determine electron density, N_e, and temperature, T_e. This is accomplished by measuring line profile appearances, including broadening and shifts, and by evaluating line ratios of specific species, respectively. When conducting experimental work associated with laser ablation in laboratory air, and here typically with pulsed laser radiation of 6 nanosecond duration, spectroscopic signatures or fingerprints of atomic species in air are clearly noticeable. The spectroscopic study of plasma emissions has evolved into a rather focused effort by many researchers around the globe recently [1, 2, 3, 4, 5, 6].

Early in the plasma decay, free electron radiation and atomic lines of hydrogen, nitrogen and oxygen dominate the emission spectra. Molecular species due to recombination occur later; however, excitation of molecular species may occur concurrent with atomic species within the first microsecond following optical breakdown. In laser ablation studies, ablated molecular species may also be discernible in the spectra. And both atomic and molecular species can be present in data records, for instance in studies of optical breakdown in methane [7] or in experimental investigations of explosive simulant with laser-induced breakdown spectroscopy (LIBS) [8].

In this work, we focus on the Balmer series of hydrogen to determine electron density in the range of 0.3×10^{17} cm^{-3} to 10×10^{17} cm^{-3}, and for temperatures typically near 10,000 K. The experimental investigations include: (1) re-evaluation of previous work of aluminum laser ablation presented in Ref. [9] and extension of electron density

analysis to utilize the peak separation as demonstrated in Ref. [10] for the hydrogen beta line at 486.14 nm. The hydrogen gamma line at 410.2 nm will be investigated for possible density diagnostics as well; and (2) simultaneous measurement of hydrogen Balmer lines subsequent to aluminum laser ablation with a thin ice layer on the surface. These studies are conducted in a collaborative effort between the University of Cairo and the University of Tennessee. The reported data were collected at the Laboratory of Laser and New Materials (LLNM) at the Faculty of Science of the University of Cairo. Concurrent efforts in laser-induced plasma studies occur at the Center for Laser Applications (CLA) of University of Tennessee Space Institute.

The electron density diagnostic standard is usually the hydrogen beta line of the Balmer series for electron densities between 10^{15} cm^{-3} to 3×10^{17} cm^{-3} [11, 12], although measurements in hydrogen gas up to $\approx 7 \times 10^{17}$ cm^{-3} [13] were reported. Detailed studies [13, 14] of laser-induced plasma show applicability of H_α to electron densities up to $\approx 10^{19}$ cm^{-3}, although self-absorption effects in laser-induced air plasma appear to be noticeable for densities $\geq 3 \times 10^{18}$ cm^{-3} [15, 16, 17]. Recent work on laser-produced hydrogen plasma [18] however addresses as $N_e^{0.70 \pm 0.03}$ and the shift as $N_e^{0.92 \pm 0.03}$.

The peak separation H_β diagnostics [10] can also be applied to determine accurately the electron density. Detailed profiles of hydrogen Balmer series lines are subject of extensive studies in the history of quantum mechanics [19] and in the study of atomic spectra [20]. The profiles computed with the standard theory are presented in so-called Stark tables [11, 12] but Stark broadening continues to be of interest from a generalized theory point of view [14]. The hydrogen beta profiles are frequently reported versus the reduced wavelength separation, α[Å], as half-width-half-maximum (HWHM). The full-width-half-maximum (FWHM), $\Delta\lambda$[nm], of the Stark-broadened hydrogen emission lines is proportional to the Holtsmark field strength, F_0, and consequently to the electron density, N_e, in units of cm^{-3}

$$\Delta\lambda[\text{nm}] = \alpha F_0 = 2.5 \times 10^{-10}\, \alpha[\text{Å}] N_e^{2/3}. \quad (1)$$

The H_β profiles show diminished contributions at line center that results in the appearance of a spectral dip. The profiles are weakly temperature dependent, but are substantially Stark broadened during the first few microseconds after laser-induced plasma generation [2, 3]. Figure 1 illustrates the H_β profiles for $N_e = 10^{17}$ cm^{-3} at $T_e = 10{,}000$ K and 20,000 K versus the reduced wavelength. For $T_e = 10{,}000$ K, the peak separation for an electron density of 10^{17} cm^{-3} equals $\Delta\lambda = 1.6$ nm, and the FWHM amounts to $\Delta\lambda = 4.6$ nm. In turn, for $T_e = 20{,}000$ K, the peak separation is 1.8 nm, and the FWHM is slightly increased to 4.8 nm. The electron density can equally be determined from computer simulations [21], that lead to a compact formulae as given in a recent review article [22], namely

$$N_e[\text{m}^{-3}] = 10^{23} \times (\Delta\lambda[\text{nm}]/4.8)^{1.46808}. \quad (2)$$

One finds for a FWHM of 4.6 nm (the $T_e = 10{,}000$ K case) the N_e value of 0.94×10^{17} cm^{-3}, and for a FWHM of 4.8 nm (the $T_e = 20{,}000$ K case) obviously from Eq. (2), $N_e = 1 \times 10^{17}$ cm^{-3}.

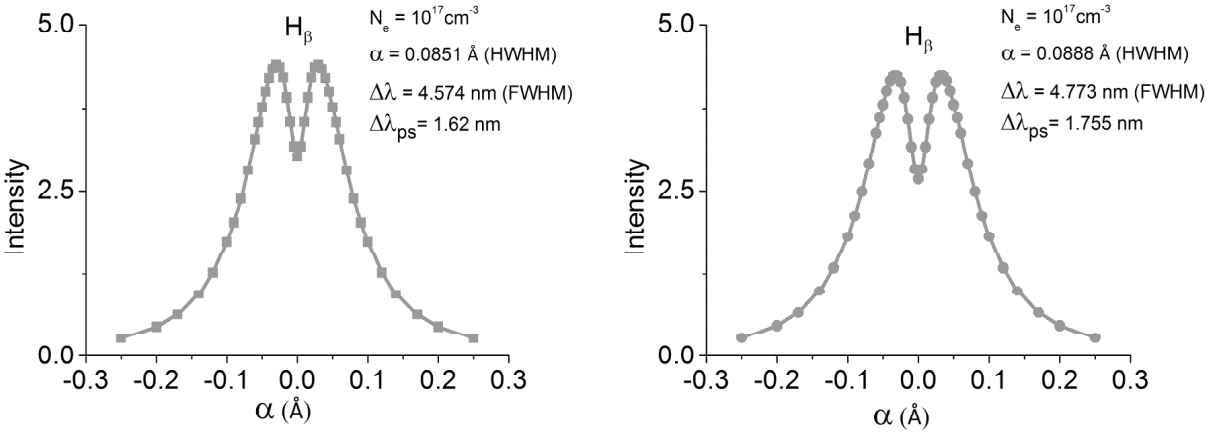

Figure 1: Left: H-beta profile for $T_e = 10{,}000$ K (squares). Right: $T_e = 20{,}0000$ K (circles). Data for the profiles are from the tables in Ref. [12], pp. 291-292

Another approximate formula, also given in a recent review article [22] for an initial N_e range of 0.5 to 3.0 × 10^{17} cm^{-3},

$$N_e[m^{-3}] = 10^{22} \times (\Delta\lambda[nm]/0.94666)^{1.49}, \quad (3)$$

is also in use for electron density determination. Results of using Equation (3) have been compared with measurements [12, 23] to be applicable for H_β up to an electron density of approximately 7 × 10^{17} cm^{-3}, and are consistent with predictions by the generalized theory of Stark broadening [14]. For the widths of 4.6 nm and 4.8 nm, corresponding to T_e of 10,000 K and 20,000 K, Eq. (3) leads to 1.05 × 10^{17} cm^{-3} and 1.12 × 10^{17} cm^{-3}, respectively.

There is a slight variation in electron density due to the differing temperatures. This variation can be nicely addressed by using the approximate formula that is also presented in the previously mentioned review article [22],

$$\log N_e[m^{-3}] = 22.578 + 1.478 \ \log \Delta\lambda[nm] - 0.144 \ (\log \Delta\lambda[nm])^2 - 0.1265 \log T_e[K]. \quad (4)$$

Equation (4) yields the identical results of N_e = 1 × 10^{17} cm^{-3} for the considered temperatures of T_e = 10,000 K and T_e = 20,000 K, see Figure 1.

The electron density can also be obtained from the peak separation [10] of the H_β line. From Equation (5) in Ref. [10],

$$\log N_e[m^{-3}] = 22.661 + 1.416 \ \log \Delta\lambda_{ps}[nm], \quad (5)$$

one finds for $\Delta\lambda_{ps}$ = 1.6 nm and $\Delta\lambda_{ps}$ = 1.8 nm the values of N_e = 0.89 × 10^{17} cm^{-3} (T_e = 10,000 K) and 1.05 × 10^{17} cm^{-3} (T_e = 20,000 K), respectively.

Figure 2 illustrates the H_δ profiles. The H_δ and H_β line profiles are displayed for identical plasma electron density, i.e., N_e = 10^{17} cm^{-3}. Yet the H_δ widths are 8.7 nm (1.9 × wider) and 9.9 nm (2.1 × wider) at T_e = 10,000 K (0.86 eV) and at T_e = 20,000 K (1.72 eV), respectively.

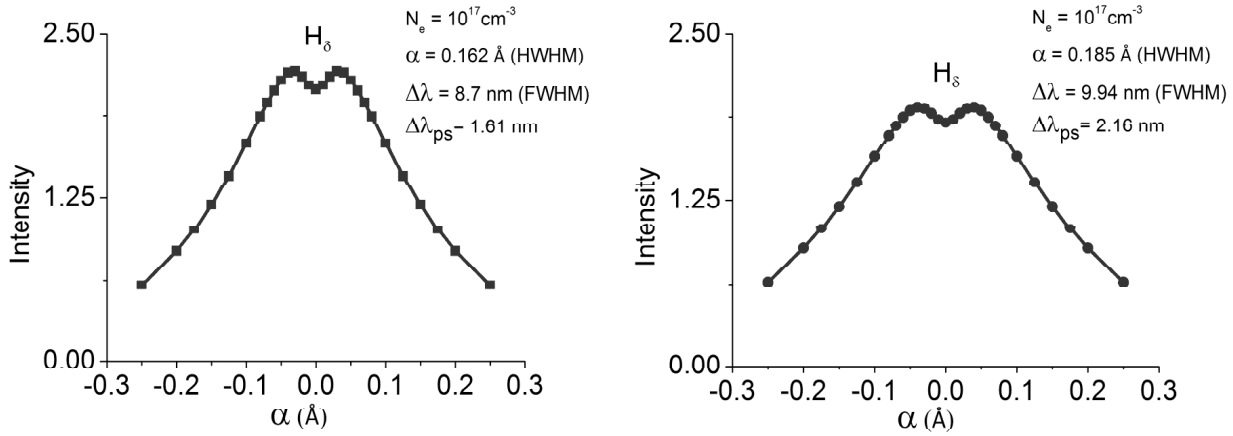

Figure 2: Left: H-delta profile for T_e = 10,000 K (squares). Right: T_e = 20,000 K (circles). Data for the profiles are from the tables in Ref. [12], p. 295

The electron density from H_α line profiles can be determined from the compact formula as presented in Ref. [22],

$$N_e[m^{-3}] = 10^{23} \times (w_{SA}[nm]/1.098)^{1.47135}, \quad (6)$$

where the full width at half area, w_{SA}. For Lorentzian line shapes including the H_α line that is close to Lorentzian for the applicability range of Equation (6), it can be justified [22] to use $w_{SA} = \Delta\lambda$.

2. EXPERIMENTAL DETAILS

In the aluminum laser ablation experiments that generate a plasma plume in air [9], the hydrogen alpha line at 656.28 nm has been used to determine the electron density from tabulated Stark profiles [11] and from the full-width at half area (FWHA) [21]. In addition, the aluminum Al II at 281.62 nm was utilized to determine the electron density. The measurements were conducted with the experimental arrangement summarized below.

Infrared, pulsed Nd:YAG radiation of 6 nanosecond duration was employed to initiate laser ablation. A 10 cm focusing lens was used to achieve a spot size of 0.5 mm, with a peak irradiance of 13×10^9 W/cm^2. The emission spectra were recorded with an echelle type spectrograph model SE 200, and an intensified charge-coupled-device (ICCD) model iStar DH734-18F. For the wavelength region of 200 nm to 1000 nm, the spectral bandwidth of the system amounted to 0.12 ± 0.02 nm over the wavelength regions of interest. The spectrograph and ICCD combination allowed one to record 40001 data points at a spacing of 0.02 nm, i.e., 6 ± 1 data points within the instrument width. An optical fiber was mounted 12.5 mm from the laser radiation axis, and 1.5 mm above the aluminum target. With this arrangement, the plasma plume emanating from the aluminum surface was studied for time delays of 10 to 0.1 μs after the laser pulse, and for electron densities of 0.6×10^{17} cm^{-3} to $\approx 10^{18}$ cm^{-3}, as indicated in Figure 8 of Ref. [9].

In this work, over and above electron density measurements using the H_β line and the Al II line, evaluation of the electron temperature T_e and further investigation of the H_β line for electron density diagnostics are of interest. Specifically, use of the peak-separation [10] and width [13] of the H_β profile is addressed. Figure 3 shows that almost the same experimental arrangement as for the aluminum laser ablation measurements in air is again assembled for laser-induced optical breakdown (LIBS) studies for aluminum laser ablation under ice, i.e., the aluminum plate is prepared with a 1 mm ice sheath.

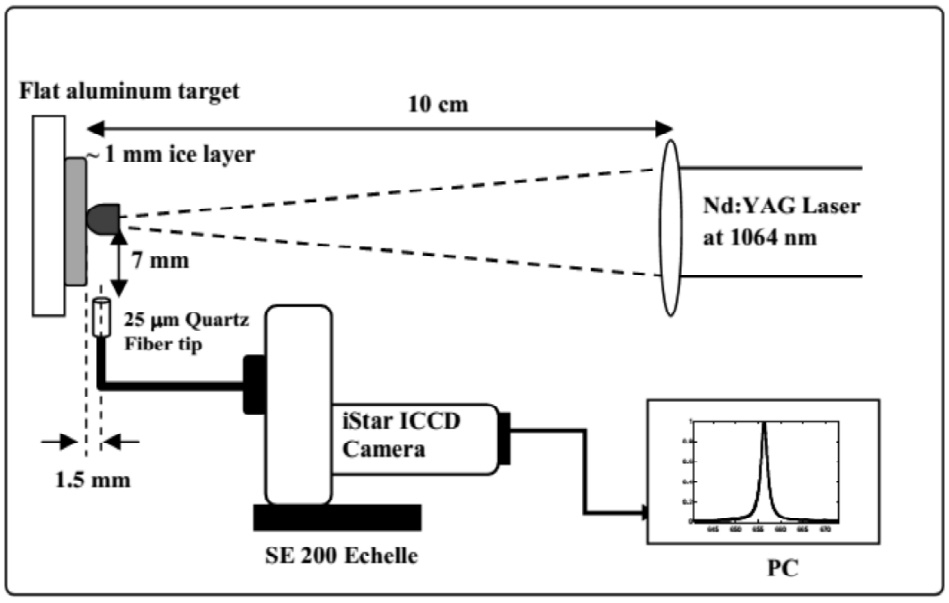

Figure 3: Experimental arrangement for measurement of plasma emissions from an ice coated target in ambient air.

3. COMPARISON WITH PREVIOUS ALUMINIUM LASER ABLATION IN AIR

The previous analysis of the laser-ablation experiments [9] focused on the determination of the electron density from the hydrogen H_α and the aluminum Al II 281.6 nm lines. Here we include, as well for reason of comparisons, the results from measurements of the Stark-broadening, $\Delta\lambda$, of the hydrogen beta line, H_β. Further, values for the electron temperature were deduced from the relative spectral intensity of H_α and H_β and were determined from the Boltzmann plots for spectral radiances of the Al II lines at the wavelengths of 281.6 nm, 358.3 nm and 466.2 nm. Table 1 shows the electron density results for time delays, $\Delta\tau$, of 1 μs to 5 μs. Table 2 shows the electron temperature as inferred from the two Balmer series lines H_α and H_β, and from aluminum Al II lines.

Table 1
Recorded Stark-broadened widths (FWHM) based on experimental data given in Ref. [9] for the indicated time delays from generation of laser-induced plasma during laser ablation. The electron densities are inferred using standard theory results [11, 12] for the H_α, H_β and the Al II line at 281.6 nm

$\Delta\tau$ [μs]	$\Delta\lambda(H_\beta)$ [nm]	$\Delta\lambda(H_\alpha)$ [nm]	½ $\Delta\lambda$(Al II) [nm]	$N_e(H_\beta)$ [10^{17} cm^{-3}]	$N_e(H_\alpha)$ [10^{17} cm^{-3}]	N_e(Al II) [10^{17} cm^{-3}]
1	18.8	4.1	0.16	7.46	7.45	7.54
2	11.5	2.6	0.08	3.61	3.76	3.77
3	10.0	2.02	0.06	2.97	2.58	2.83
4	8.9	1.65	0.05	2.50	1.90	2.35
5	6.4	1.37	0.03	1.52	1.44	1.41

Table 2
Inferred electron temperatures T_e for the indicated time delays including use of optically thin spectral intensities of the Al II lines at 281.6 nm, 358.3 nm and 466.3 nm lines

time delay, $\Delta\tau$ [μs]	T_e from H_α and H_β [K]	T_e from Al II lines [K]
1	13,000	12,600
2	10,000	10,000
3	8,700	9,000
4	8,100	8,100
5	7,400	7,800

The previously recorded spectral signatures near the H_γ and H_δ lines show significant interference due to presence of other species. Analysis of the H_δ profiles would also be challenging due to the low signal, and the expected weakly developed peak separations. However, the results of analyses based on the hydrogen beta Balmer series line peak-separation [10] are also reported in Table 3. As the electron density increases, the double peak structure becomes asymmetric with a stronger peak towards the Ultra-Violet. Aluminum laser-ablation experiments [24] in a hydrogen gas environment also indicates this trend.

Table 3
Hydrogen beta line peak-separation as deduced from data in Ref. [9], and inferred electron density using recently published results [10], see Eq. (5)

time delay, $\Delta\tau$[μs]	peak separation, $\Delta\lambda_{ps}$ [nm]	electron density, N_e [10^{17} cm^{-3}]
1	6.0	6.4
2	4.3	3.9
3	3.2	2.5
4	2.5	1.8
5	2.1	1.4

The peak separations for the previously recorded H_β line profiles show at least an error of 20%, and with the error propagation factor of ≈ 1.5 (see Eq. (5)), the electron density will have an error of about 30%. Yet the determined electron density values from the hydrogen alpha width (compare Table 1) and from the peak separations appear to agree within the error bars.

Following the initial re-analysis of the previous laser-ablation experiments [9], with focus on H_β line profiles in this work, an effort was made to increase the signal-to-noise ratio of the hydrogen beta and hydrogen delta lines.

Laser-induced plasma is generated in presence of water vapor and subsequently during aluminum laser-ablation under ice.

4. RESULTS FOR ALUMINUM LASER ABLATION UNDER ICE

In our study, laser-induced emission spectra were collected first in water-vapor for the following reasons: (a) measurement with an increased signal-to-noise ratio particularly for the H_β, H_γ and H_δ lines; (b) investigation of the appearances of the H_β and H_δ lines; (c) establishment of a reference spectrum for experiments of laser-ablation under ice. Figure 4 shows a typical recorded spectrum for a time delay of 2 μs after generation of optical breakdown. The data were collected using a gate-width of 1 μs. The figure shows both the original "noisy" data and 101 points, 2-nd order Savitzky-Golay filter that was applied to possibly extract the lower-frequency peaks for the H_β and H_δ profiles. Note that there appears to be a spectral interference for the H_δ line. Figure 4 also displays the H_α line region of the recorded spectrum.

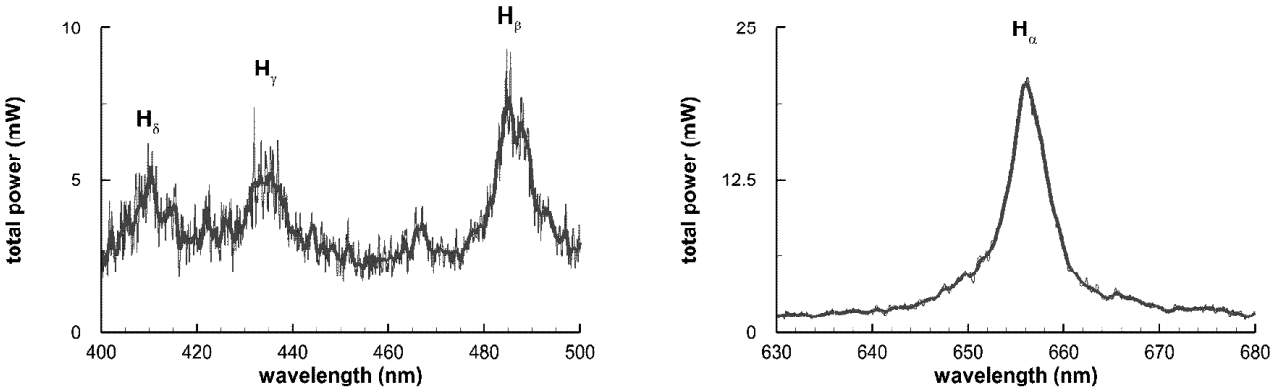

Figure 4: Left: H_β, H_γ and H_δ line profiles in the 400 nm to 500 nm region. Right: H_α line profile in the 630 nm to 680 nm region of the same data set recorded from laser-induced plasma in water vapor. Time delay 2 μs, gate width 1 μs.

Due to the spectral interference near the H_γ and H_δ lines in the water vapor experiments, H_γ and H_δ for laser ablation diagnostics is expected to be of lesser value than H_α and H_β diagnostics.

The emission spectra from pulsed laser ablation under ice were collected systematically for time delays of 0 μs to 5 μs in 1 μs steps. A gate width of 1 μs was selected for these measurements. The experimental arrangements for the investigations under an ice sheath, illustrated in Figure 3, are similar to previously communicated studies of laser ablation in air [9]. The work reported here focuses on applicability of the hydrogen Balmer series diagnostics for description of laser-ablation. A total of 100 individual events were collected with the echelle spectrograph and intensified CCD camera.

The recorded data were wavelength calibrated and detector sensitivity corrected. For the detector sensitivity, an absolute calibration in terms of Watts/detector-count was performed using the DH2000-CAL tungsten halogen lamp at the LLNM of Cairo University. The spectra were digitally filtered at CLA of the the University of Tennessee Space Institute using a 51-point, 2-nd order Savitzky-Golay filter. Figures 5 to 7 display the recorded data for time delays of 1 μs to 5 μs and for the wavelength range of 400 nm to 500 nm.

For time delays longer than ≈ 1 μs, the H_β line can be recognized and it shows the expected double peak structure and/or dip at line center for time delays ≥ 2 μs. Also, the H_γ line profile at 434.0 nm can be identified but other spectroscopic features indicative of molecular bands appear in the H_γ wavelength region. The H_δ line profile appears to be masked by other spectroscopic features. These features appear as blue-degraded bands but are not further identified here. Pulsed laser ablation studies in air typically show rich atomic and molecular emissions, e.g., for carbon containing samples [25]. The H_γ and H_δ line profiles certainly show spectroscopic interference, consequently, laser-ablation electron density diagnostics with H_γ and H_δ lines is avoided for the indicated time

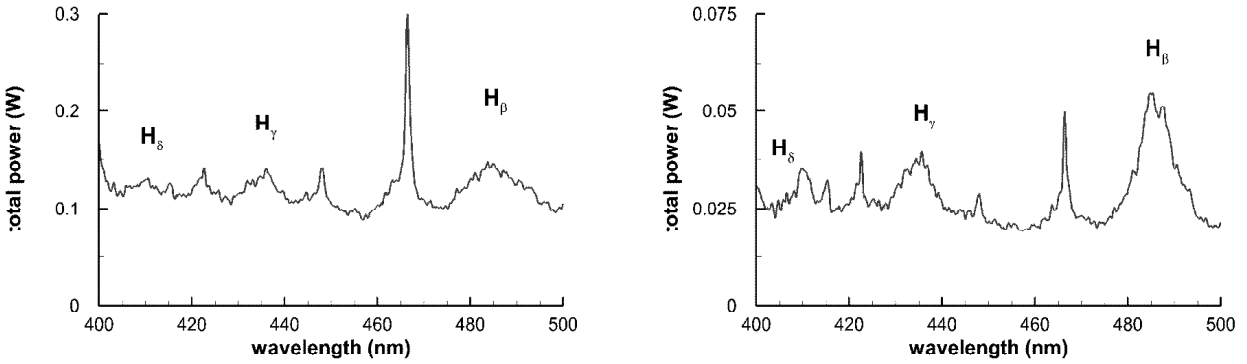

Figure 5: Time delays (left) Δτ = 1 μs and (right) Δτ = 2 μs, gate-width 1 μs.

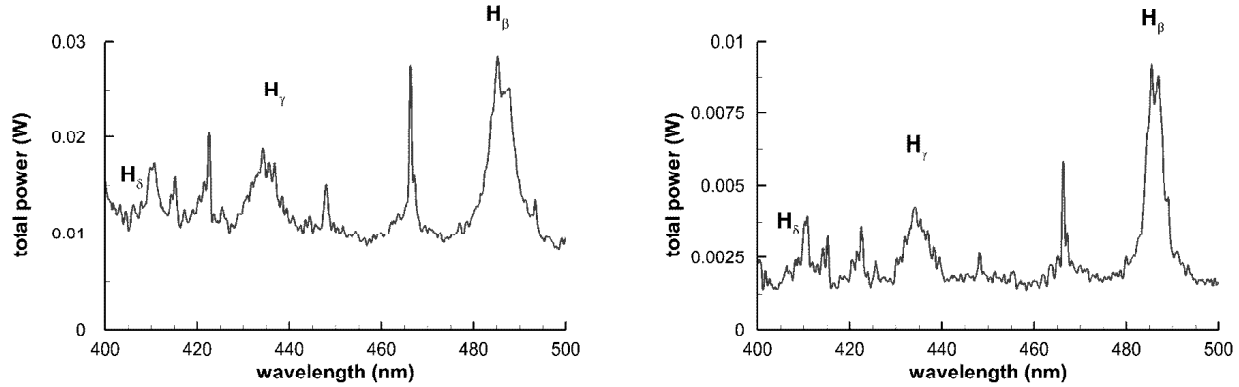

Figure 6: Time delays (left) Δτ = 3 μs and (right) Δτ = 4 μs, gate-width 1 μs.

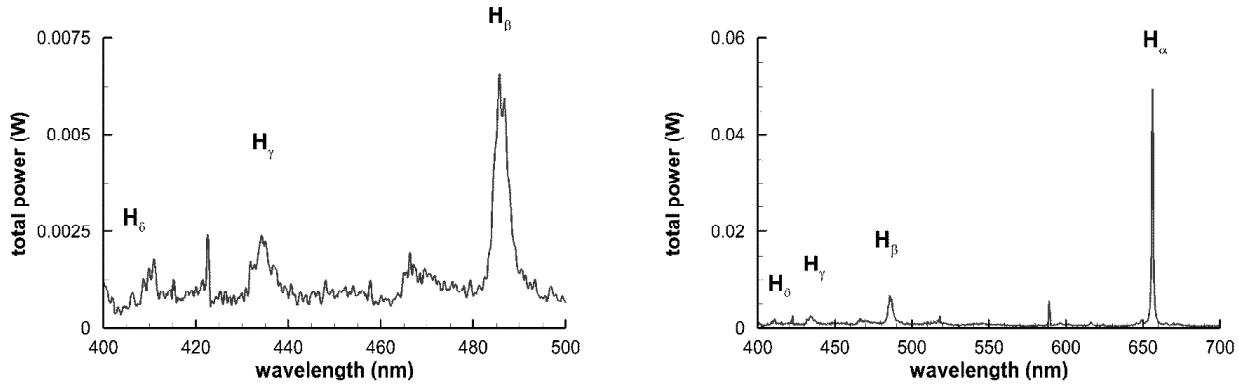

Figure 7: Time delay Δτ = 5 μs, gate-width 1 μs. Left: 400 nm to 500 nm. Right: 400 nm to 700 nm. The expanded view on the right also shows the sodium D-lines at 589 nm and 589.6 nm.

delays of up to 5 μs following laser-ablation under ice. Table 4 shows the measured widths and inferred electron densities.

For the 1 μs data, the H_β results in the round brackets indicate only estimates for widths and the peak separation, see Figure 5. The results for the H_β from width and peak separation lead to consistent electron densities. Recently, spatially resolved measurements were reported that characterize aluminum plasma with the Thomson scattering technique [26]. Laser ablation of an aluminum target was used to generate the plasma in ambient air leading to electron densities in the range of 3.4×10^{17} cm^{-3} to 0.5×10^{17} cm^{-3} for time delays of 0.6 μs to 3 μs, respectively.

Table 4: H_β widths, peak separations, H_α widths for aluminum laser ablation under ice, and determined electron densities including results for the Al II line at 281.6 nm

$\Delta\tau$ [μs]	$\Delta\lambda(H_\beta)$ [nm]	$\Delta\lambda_{ps}(H_\beta)$ [nm]	$\Delta\lambda(H_\alpha)$ [nm]	$N_e(\Delta\lambda(H_\beta))$ [10^{17} cm^{-3}]	$N_e(\Delta\lambda_{ps}(H_\beta))$ [10^{17} cm^{-3}]	$N_e(\Delta\lambda(H_\alpha))$ [10^{17} cm^{-3}]	$N_e(\Delta\lambda(Al\ II))$ [10^{17} cm^{-3}]
1	(22)	(6.5)	4.2	(18.6)	(6.3)	7	5.9
2	9.9	3.8	2.3	5.7	2.9	3.13	3.3
3	5.4	3	1.7	2.35	2	1.99	2.3
4	3.8	2.25	1.1	1.4	0.75	1.28	2.1
5	2.8	1.25	0.9	0.9	0.57	1.0	–

5. DISCUSSION

Our interest is primarily in the study of emission spectra in the optical region that is usually of interest in laser-induced breakdown spectroscopy (LIBS). The spectrally well-separated and strong hydrogen alpha line at 656.28 nm appears to be very useful for the determination of electron densities in pulsed laser ablation in air and for electron densities in the range of 10^{17} cm^{-3} to 10^{18} cm^{-3}. We find in this work that the peak separation of the hydrogen beta line can yield [27] accurate results for electron densities on the order of up to $\approx 5 \times 10^{17}$ cm^{-3} , consistent with the well-documented accuracy of the hydrogen beta line for plasma diagnosis.

The laser-ablation plasma spectra in the region of the first four atomic lines of hydrogen, i.e., H_α, H_β, H_γ, and H_δ, were recorded in the plume emanating from the sample but with fiber-optic collection slightly displaced from the surface. At this location, hydrogen Balmer series diagnostics works well for electron densities $\leq 10 \times 10^{17}$ cm^{-3}. The line-of-sight measurements represent an average of the electron density and temperature, consequently it will be of interest to spatially resolve the plasma plume. Moreover, smaller gate widths will be of interest in future work to possibly extend H_α laser ablation diagnostics applications. Electron densities well in excess of 3×10^{18} cm^{-3} are usually encountered close to the surface.

Acknowledgments

We thank for support in part by a travel grant for CGP by the University of Cairo and for support in part by The Center for Laser Applications of The University of Tennessee Space Institute.

References

[1] L. Radziemski, and D. Cremers, editors, *Laser-induced plasmas and applications*, M. Dekker, New York, 1989.

[2] A. Miziolek, V. Palleschi, and I. Schechter, editors, *Laser Induced Breakdown Spectroscopy*, Cambridge University Press, New York, 2006.

[3] D. Cremers, and L. Radziemski, *Handbook of Laser-Induced Breadkown Spectroscopy*, John Wiley, New York, 2006.

[4] J. Singh, and S. Thakur, editors, *Laser Induced Breakdown Spectroscopy*, Elsevier Science, New York, 2007.

[5] R. Noll, *Laser-Induced Breakdown Spectroscopy*, Springer, Heidelberg, 2011.

[6] S. Musazzi, and U. Perini, editors, *Laser-Induced Breakdown Spectroscopy*, Springer, Heidelberg, 2014.

[7] C. G. Parigger, A. Woods, and J. O. Hornkohl, *Appl. Opt.* **51**, B1–B6 (2012).

[8] M. J. Witte, C. G. Parigger, N. A. Bullock, J. A. Merten, and S. D. Allen, *Appl. Spectrosc.* **68**, 367–370 (2014).

[9] A. M. El Sherbini, H. Hegazy, and Th. M. E Sherbini, *Spectrochim. Acta Part B* **61**, 532–539 (2006).

[10] M. Ivković, N. Konjević, and Z. Pavloviæ, *J. Quant. Spectrosc. Radiat. Transf.* **154**, 1–8 (2015).

[11] H. R. Griem, *Plasma Spectroscopy*, McGraw-Hill Book Company, New York, 1964.

[12] H. R. Griem, *Spectral Line Broadening by Plasmas*, Academic Press, New York, 1974.

[13] C.G. Parigger, D. H. Plemmons, and E. Oks, *Appl. Opt.* **42**, 5992–6000 (2003).

[14] E. Oks, *Stark Broadening of Hydrogen and Hydrogenlike Spectral Lines in Plasmas, The Physical Insight*, Alpha Science, 2006.

[15] C. G. Parigger, L.D. Swafford, D. M. Surmick, M.J. Witte, A.C. Woods, and G. Gautam, *J. Phys: Conf. Ser.* **548**, 012042 (2014).

[16] L.D. Swafford, D.M. Surmick, M.J. Witte, A.C. Woods, G. Gautam, and C.G. Parigger, *J. Phys: Conf. Ser.* **548**, 012049 (2014).

[17] C. Parigger, G. Gautam, A. Woods, D. Surmick, and J. Hornkohl, *Trends Appl. Spectrosc.* **11**, (in press) (2014).

[18] J. F. Kielkopf, and N. F. Allard, *J. Phys. B: At. Mol. Opt. Phys.* **47**, 155701 (2014).

[19] E. Schrödinger, *Phys. Rev.* **28**, 1049–1070 (1926).

[20] E. U. Condon, and G. H. Shortley, *The Theory of Atomic Spectra*, Cambridge University Press, New York, 1953.

[21] M. Gigosos, M. González, and V. Cardeñoso, *Spectrochim. Acta Part B* **58**, 1489–1504 (2003).

[22] N. Konjević, M. Ivković, and N. Sakan, *Spectrochim. Acta Part B* **76**, 16–26 (2012).

[23] C. G. Parigger, *Spectrochim. Acta Part B* **79-80**, 4–16 (2013).

[24] C. G. Parigger, J. O. Hornkohl, and L. Nemes, *Appl. Opt.* **46**, 4026–4031 (2007).

[25] J. J. Camacho, L. Díaz, M. Santos, D. Reyman, and J. M. L. Poyato, *J. Phys. D: Appl. Phys* **41**, 105201 (2008).

[26] A. Mendys, M. Kañski, A. Farah-Sougueh, S. Pellerin, B. Pokrzywka, and K. Dzierżęga, *Spectrochim. Acta Part B* **96**, 61–68 (2014).

[27] G. Gautam, D. M. Surmick, and C. G. Parigger, *J. Quant, Spectrosc. Radiat, Transf.* **160**, 19-21 (2015).